

PM/98-08
 THES-TP 98/04
 hep-ph/9803422
 March 1998

Testing the Higgs boson gluonic couplings at LHC[†]

G.J. Gounaris^a, J. Layssac^b and F.M. Renard^b

^aDepartment of Theoretical Physics, University of Thessaloniki,
 Gr-54006, Thessaloniki, Greece.

^bPhysique Mathématique et Théorique, UMR 5825
 Université Montpellier II, F-34095 Montpellier Cedex 5.

Abstract

We study Higgs + jet production at hadron colliders in order to look for new physics residual effects possibly described by the $dim = 6$ operators \mathcal{O}_{GG} and $\tilde{\mathcal{O}}_{GG}$ which induce anomalous Hgg and $Hggg$ couplings. Two ways for constraining these operators at LHC may be useful. The first is based on the total Higgs boson production rate induced by gluon-gluon fusion, in which the main cause of limitations are due to theoretical uncertainties leading to sensitivities of $|d_G| \simeq 3. \times 10^{-4}$ and $|\tilde{d}_G| \simeq 1.4 \times 10^{-3}$ for the corresponding anomalous couplings, in the mass range $100 \text{ GeV} \lesssim m_H \lesssim 200 \text{ GeV}$. These results imply sensitivity to new physics scales of 51 and 24 TeV respectively. The second way investigated here concerns the shape of the Higgs transverse momentum; for which the theoretical uncertainties are less severe and the limitations are mainly induced by statistics. A simple analysis, based on the ratio of the number of events at large and low p_T at LHC, leads to similar sensitivities, if only the $H \rightarrow \gamma\gamma$ decay mode is used. But the sensitivities can now be improved by a factor 2 to 10, depending on the Higgs mass, if the Higgs decay modes to WW^* , ZZ^* , WW , ZZ are also used.

[†]Partially supported by the EC contract CHRX-CT94-0579.

1 Introduction

The Higgs mechanism is the cornerstone of the Standard Model (SM) [1]. Much experimental and theoretical effort has already been done to discover the Higgs boson, and to understand the origin of the scalar sector and constrain the Higgs boson mass, which is to a large extent arbitrary. At present, the negative experimental searches at LEP2 lead to the conclusion that $m_H \gtrsim 77$ GeV [2], while precision measurements at Z peak give $m_H = 115^{+116}_{-66}$ GeV within the SM context [3]. These values are well within the bounds obtained from purely theoretical considerations [4].

Searches are presently going on at LEP2 and the Tevatron and will be pursued at LHC. If the Higgs boson is light, its discovery should be at hand. However, such a discovery, will only constitute the first step in the study of the scalar sector. Detailed studies of the properties of the Higgs candidate should then be performed aiming at first confirming the Higgs nature, and then trying to get information about the origin of the scalar sector. This origin may very well lie in an underlying fundamental dynamics generically called new physics (NP).

Assuming that the NP degrees of freedom are associated to an energy scale Λ_{NP} much larger than any conceivably accessible energy range, any observable NP manifestation could only be in the form of residual effects modifying the SM interactions among usual particles and the (yet to be discovered) Higgs boson. At the energy range of the foreseeable colliders, the leading such effects may arise from the set of $dim = 6$ $SU(3) \times SU(2) \times U(1)$ gauge invariant operators [5, 6, 7], involving an isodoublet Higgs field and the particles with the highest affinity to it, which inspired by SM, are taken to be the quarks of the third family. Of course, apart from these fields, the NP operators necessarily also involve gauge bosons, inevitably introduced by the gauge principle whenever a derivative appears. The complete list of the CP conserving such operators has been given in [6, 7], while the CP violating ones have appeared in [8, 9]. Tests of their effects at present and future colliders have been given for most of them in [6, 7, 10, 11, 12, 13].

Among these operators, those inducing anomalous Higgs-gluon couplings beyond the SM ones arise when the NP degrees of freedom are coloured. Examples of dynamical models in which such operators are generated have been pointed out [6], but very little has yet been said about their possible signatures [14].

The aim of this paper is to study the Higgs-gluon couplings induced by these operators, namely the CP-conserving one dubbed \mathcal{O}_{GG} and its CP-violating analogue $\tilde{\mathcal{O}}_{GG}$, respectively associated to dimensionless couplings d_G and \tilde{d}_G . These operators are the gluonic analogues of the operators \mathcal{O}_{BB} , \mathcal{O}_{WW} , $\tilde{\mathcal{O}}_{BB}$ and $\tilde{\mathcal{O}}_{WW}$, which are inducing anomalous Higgs couplings to the electroweak gauge bosons and have been studied in [15, 16, 17, 9]. Since the SM couplings among Higgs bosons and gluons, first appear only at the 1-loop level, (essentially through a top quark loop), and are therefore somewhat reduced, there is a favorable situation for the detection of any NP contribution induced at tree level by the possible operators \mathcal{O}_{GG} and $\tilde{\mathcal{O}}_{GG}$. Other types of NP effects, like *e.g.* the anomalous g_{tt} and H_{tt} couplings modifying the Hgg and Hg_{gg} interactions through a top-loop contribution, may also appear, [18]. Below, we show how the presence of these NP effects

can be tested through studies of Higgs boson production and decay.

As the $H \rightarrow gg$ branching ratio only represents a small fraction (6-7% for $m_H \simeq 100 - 150$ GeV and much less for higher masses), accurate measurements of the Hgg couplings through decay width $\Gamma(H \rightarrow gg)$ will need a copious Higgs boson production and very powerful methods for distinguishing gg from light quark final states. At e^+e^- colliders, only a few $H \rightarrow gg$ events are expected through HZ production; *i.e.* a few tens at LEP2 and a few hundreds at a higher energy linear collider (LC), depending on the achieved luminosity. An analysis based on a luminosity of 50 fb^{-1} at a 500 GeV LC, led to an uncertainty of $\pm 39\%$ for the sum $c\bar{c} + gg$ [19]. The same situation probably also arises for H production in a $\gamma\gamma$ Collider. At the upgraded Tevatron, a hundred of Higgs particles should be produced (mainly through the process $p\bar{p} \rightarrow WH + X$) for $m_H \simeq 100 - 150$; but its observation seems possible only in the $b\bar{b}$ mode [20].

The situation should be quite different at LHC where a copious Higgs production of about $10^5 - 10^6$ events per year for $m_H \lesssim 200 \text{ GeV}$, should be expected [21, 22, 23, 24, 25]. At the LHC energies, the largest cross sections arise from subprocesses with gg , WW/ZZ and $q\bar{q}$ initial states, as well as from bremsstrahlung off a top quark. Among these, the process $gg \rightarrow H$ largely dominates. So this should be the best place to look for anomalous Hgg , $Hggg$ couplings. The standard prediction for this process has been computed and found very sensitive to higher order QCD corrections due to soft gluon effects, for the resummation of which there exist large theoretical uncertainties [26, 27]. This means that an accurate measurement of Hgg couplings through the total production rate is only hindered by theoretical uncertainties, while statistics are enormous. Assuming a conservative theoretical error for the QCD corrections, we estimate the discovery limits for the \mathcal{O}_{GG} and $\tilde{\mathcal{O}}_{GG}$ effects. These limits are interesting, since they correspond to NP scales lying in the tens of TeV range.

A theoretically cleaner (and in any case complementary) study of the operators \mathcal{O}_{GG} and $\tilde{\mathcal{O}}_{GG}$ could be achieved by looking at the Higgs transverse momentum distribution in the $Higgs + jet$ production process. To our knowledge, this has never been discussed before for the search of NP effects. To achieve this, one first needs the 1-loop SM amplitudes for $gg \rightarrow Hg$, $gq \rightarrow Hq$ and $q\bar{q} \rightarrow Hg$, that will interfere with the NP ones. These SM contributions have been computed in [28, 29]. We have recomputed them and checked numerically the agreement with the results obtained previously. Adding then the NP contributions due to the operators \mathcal{O}_{GG} and $\tilde{\mathcal{O}}_{GG}$, we have examined how the SM predictions for the various observables, (like *e.g.* the distributions of the Higgs rapidity and transverse momentum, and the Higgs+jet invariant mass and angular distributions) are influenced by NP.

The most striking effect is, as expected, in the p_T dependence. The SM prediction (as well as the one of any other NP model affecting only ggt and Htt couplings) should drop down as soon as $p_T \gtrsim m_t$; whereas the NP contribution due to \mathcal{O}_{GG} and $\tilde{\mathcal{O}}_{GG}$ operators (associated to a heavy Λ_{NP}) stays flat, leading to a clear signal for anomalous couplings. We then derive the observability limits on d_G and \tilde{d}_G by considering the ratio of Higgs+jet production rates, at the high and low p_T regions.

The content of the paper is the following. In Section 2 we present the \mathcal{O}_{GG} and $\tilde{\mathcal{O}}_{GG}$

operators and derive the unitarity constraints relating the NP couplings to the scale Λ_{NP} , where the new degrees of freedom start being excited. We then present the formulae for the NP and SM contributions to the $H \rightarrow gg$ decay, and to the Higgs boson and $H + jet$ production in pp collisions. The sensitivity limits to the NP couplings are derived in Section 3, first on the basis of the expected accuracy in the measurement of the $\Gamma(H \rightarrow gg)$ width; and then on the basis of the Higgs production rate and the various $H + jet$ distributions at LHC. We find that for $100 \lesssim m_H \lesssim 200\text{GeV}$, the study of the total Higgs production rate, and the study of the p_T -distribution in the case that only $H \rightarrow \gamma\gamma$ is used for H -detection, give comparable results. On the other hand the p_T -distribution technique starts becoming superior whenever the $H \rightarrow WW^*$, ZZ^* , WW , ZZ decay modes are also used to increase its statistics, which may even lead to an order of magnitude improvement as m_H approaches the 200 GeV region. Section 4 summarizes the results and their implications for the NP search. Technical details on invariant amplitudes, loop computations and parton kinematics are collected in an appendix.

2 Formalism.

2.1 The NP operators \mathcal{O}_{GG} and $\tilde{\mathcal{O}}_{GG}$.

We consider the NP effects arising from the effective Lagrangian

$$\mathcal{L}_{NP} = \frac{d_G}{v^2} \mathcal{O}_{GG} + \frac{\tilde{d}_G}{v^2} \tilde{\mathcal{O}}_{GG} , \quad (1)$$

where d_G and \tilde{d}_G are NP dimensionless couplings, and the NP operators are

$$\mathcal{O}_{GG} = \left(\Phi^\dagger \Phi - \frac{v^2}{2} \right) \vec{G}_{\mu\nu} \cdot \vec{G}^{\mu\nu} , \quad (2)$$

$$\tilde{\mathcal{O}}_{GG} = (\Phi^\dagger \Phi) \vec{\tilde{G}}_{\mu\nu} \cdot \vec{G}^{\mu\nu} , \quad (3)$$

with $\tilde{G}_{\mu\nu}^i \equiv 1/2\epsilon_{\mu\nu\lambda\sigma}G^{i\lambda\sigma}$ and

$$\Phi = \begin{pmatrix} i\chi^+ \\ \frac{1}{\sqrt{2}}(v + H - i\chi^3) \end{pmatrix} . \quad (4)$$

Unitarity allows to establish for each operator an unambiguous relation between the NP coupling constants appearing in (1), and the corresponding energy scale Λ_{NP} , at which unitarity is saturated. This scale supplies a practical definition of the scale where the new physics generates the corresponding operator [6, 30, 16].

In the case of the \mathcal{O}_{GG} and $\tilde{\mathcal{O}}_{GG}$ operators, the strongest unitarity constraint arises from the $J = 0$ partial wave transition amplitude affecting the colour singlet channels $|gg \pm \pm\rangle$ and $|HH\rangle$. Using (1), we thus get for \mathcal{O}_{GG} the unitarity relation

$$d_G = \frac{4\pi}{1 + c \frac{\pi v^2}{\Lambda_{NP}^2}} \left(\frac{v^2}{\Lambda_{NP}^2} \right) \quad (5)$$

with $c = 31$ for $d_G > 0$, and $c = -1$ for $d_G < 0$. The unitarity relation for $\tilde{\mathcal{O}}_{GG}$ is

$$|\tilde{d}_G| = \frac{4\pi}{1 + 15\frac{\pi v^2}{\Lambda_{NP}^2}} \left(\frac{v^2}{\Lambda_{NP}^2} \right) . \quad (6)$$

2.2 The $H \rightarrow gg$ decay width

In this section we give the modification to the Higgs gluonic decay width induced by tree level effects of the operators \mathcal{O}_{GG} and $\tilde{\mathcal{O}}_{GG}$.

The Hgg gauge-invariant amplitude¹ $R(Hgg)$ is given by

$$R(Hgg) = if(k^2)\delta_{ab}[(k.k')(\epsilon.\epsilon') - (\epsilon.k')(\epsilon'.k)] , \quad (7)$$

where the gluon momenta and polarization vectors are denoted as (k, ϵ) and (k', ϵ') respectively². In (7), the momentum k is allowed to be off-shell, while the other gluon with momentum k' and polarization ϵ' is always on-shell. Under such conditions, there is only one gauge invariant form for Hgg , which is shown in (7). The indices (a, b) specify the colours of the two gluons. In SM, the dominant contribution arises from the top triangle in Fig.1a and is given by

$$f(k^2) = \frac{\alpha_s m_t^2}{\pi v} \bar{f}(k^2) , \quad (8)$$

in terms of $\bar{f}(k^2)$ presented in Appendix A1. Here we only note that $f(0)$ agrees with the result quoted in [23, 24, 26, 28, 29]. In the heavy quark limit $m_t \gg m_H$, this leads to the well known result [31, 29]

$$\bar{f}(0) \rightarrow -\frac{1}{3m_t^2} . \quad (9)$$

In the presence of the NP contribution given in (1), the Higgs decay width into 2 real gluons is given by

$$\Gamma(H \rightarrow gg) = \frac{m_H^3}{8\pi} \left\{ |f(0) - \frac{4d_G}{v}|^2 + \frac{16}{v^2} |\tilde{d}_G|^2 \right\} . \quad (10)$$

As expected, only the CP-conserving NP contribution interferes with the SM one.

2.3 Higgs and Higgs+jet production at pp colliders

2.3.1 Single Higgs production

At lowest QCD order, including the effect of the NP operators \mathcal{O}_{GG} and $\tilde{\mathcal{O}}_{GG}$, the total rate for $pp \rightarrow H + X$ due to the subprocess $gg \rightarrow H$ is given by

$$\sigma^0(pp \rightarrow H + X) = \hat{\sigma}^0 \tau_H L_{gg} , \quad (11)$$

¹The phase of the amplitude is defined to be that of the S -matrix element.

²All momenta are taken as incoming.

where

$$L_{gg} = \int_{\tau_H}^1 \frac{dx}{x} g(x) g\left(\frac{\tau_H}{x}\right) , \quad (12)$$

$$\hat{\sigma}^0 = \frac{\pi^2}{8m_H^3} \Gamma(H \rightarrow gg) = \frac{\pi}{64} \left\{ |f(0) - \frac{4d_G}{v}|^2 + \frac{16}{v^2} |\tilde{d}_G|^2 \right\} , \quad (13)$$

$\tau_H = m_H^2/s$ and $g(x)$ is the gluon distribution function inside the proton.

QCD corrections correspond to including loop corrections to $gg \rightarrow H$, as well as corrections due to associated production of massless partons together with the Higgs, in the processes $gg \rightarrow Hg$, $q\bar{q} \rightarrow Hg$, $gq \rightarrow Hq$, $g\bar{q} \rightarrow H\bar{q}$ [21, 22, 32, 24, 27, 26, 33]. The result in SM is

$$\sigma(pp \rightarrow H + X) = \hat{\sigma}^0 \left[1 + C \frac{\alpha_s}{\pi} \right] \tau_H L_{gg} + \Delta\sigma_{gg} + \Delta\sigma_{gq} + \Delta\sigma_{g\bar{q}} + \Delta\sigma_{q\bar{q}} \quad (14)$$

where the various terms correspond to gg , $gq(\bar{q})$ and $q\bar{q}$ initial state. Depending on the value of the Higgs mass, these QCD corrections increase the Higgs production rate by 60% to 90% [21, 32, 24, 26, 27, 33].

2.3.2 H+jet production at large p_T .

We now turn to Higgs + jet production (Fig.2), which at a hadron collider, takes place through the subprocesses (Fig.3) $gg \rightarrow Hg$, $gq \rightarrow Hq$, $g\bar{q} \rightarrow H\bar{q}$, $q\bar{q} \rightarrow Hg$ [28, 29].

We have repeated the computation of [29] of the triangle and box contributions to the various types of subprocesses participating in the $H + jet$ production (compare Fig.3), and we have added the tree level NP contributions due to \mathcal{O}_{GG} and $\tilde{\mathcal{O}}_{GG}$. The \mathcal{O}_{GG} contribution interferes with SM, whereas the $\tilde{\mathcal{O}}_{GG}$ one does not and adds quadratically in the cross section.

Details on the amplitudes are given in Appendix A2; while those on the kinematics of the two-body inclusive parton model distributions, are presented in Appendix A3. We collect there the expressions for the Higgs transverse momentum distribution $d\sigma/dp_T$, the H rapidity distribution $d\sigma/dy_H$, the (H+jet) invariant mass distribution $d\sigma/dM$, and the angular distribution $d\sigma/d\chi$. They are obtained by convoluting the elementary differential cross section $d\hat{\sigma}/d\hat{t}$ for the various subprocesses, with gluon and quark distributions.

For $gg \rightarrow Hg$ the elementary differential cross section is

$$\begin{aligned} \frac{d\hat{\sigma}(gg \rightarrow Hg)}{d\hat{t}} = & \frac{3\hat{u}\hat{t}}{128^2\pi\hat{s}} \left\{ (\hat{u}\hat{t})^2 \left(|A_1|^2 + \frac{\hat{s}^2}{2} |A_4|^2 \right) + 4(|A_2|^2 \hat{u}^2 + |A_3|^2 \hat{t}^2) \right. \\ & - 4\hat{u}\hat{t}\Re(A_2 A_3^*) + 2\hat{u}\hat{t}\Re((\hat{t}A_3 - \hat{u}A_2)(A_1^* + \hat{s}A_4^*)) + \hat{s}(\hat{t}\hat{u})^2 \Re(A_1 A_4^*) \Big\} \\ & + \frac{3\alpha_s |\tilde{d}_G|^2}{8v^2} \left[\frac{2p_T^2}{\hat{s}^2} - \frac{4}{\hat{s}} \left(1 - \frac{M_H^2}{\hat{s}} \right)^2 + \frac{1}{p_T^2} \left(\left(1 - \frac{M_H^2}{\hat{s}} \right)^4 + 1 + \left(\frac{m_H^2}{\hat{s}} \right)^4 \right) \right] \end{aligned} \quad (15)$$

In this expression the functions A_i contain both SM and \mathcal{O}_{GG} contributions as given by (A.18, A.19, A.13, A.14) in the Appendix A2. The quantity p_T denotes the transverse Higgs

momentum; compare Appendix A3. As expected, the CP-violating $\tilde{\mathcal{O}}_{GG}$ contributions does not interfere with SM and appear separately in quadratic form. This \tilde{d}_G quadratic term is the same as the quadratic term of the \mathcal{O}_{GG} contribution (coming from the functions A_i) by just replacing $d_G \rightarrow \tilde{d}_G$.

While for $q\bar{q} \rightarrow Hg$ and $gq(\bar{q}) \rightarrow Hq(\bar{q})$ we get

$$\frac{d\hat{\sigma}(q\bar{q} \rightarrow Hg)}{d\hat{t}} = \frac{\alpha_s}{36\hat{s}^3}(\hat{t}^2 + \hat{u}^2) \left\{ |f(\hat{s}) - \frac{4d_G}{v}|^2 + \frac{16}{v^2}|\tilde{d}_G|^2 \right\} , \quad (16)$$

$$\frac{d\hat{\sigma}(gq \rightarrow Hq)}{d\hat{t}} = \frac{d\hat{\sigma}(g\bar{q} \rightarrow H\bar{q})}{d\hat{t}} = \frac{\alpha_s}{96\hat{s}^2|\hat{t}|}(\hat{s}^2 + \hat{u}^2) \left\{ |f(\hat{t}) - \frac{4d_G}{v}|^2 + \frac{16}{v^2}|\tilde{d}_G|^2 \right\} . \quad (17)$$

The corresponding expressions for $\bar{q}q \rightarrow Hg$, $qg \rightarrow Hq$, $\bar{q}g \rightarrow H\bar{q}$ are obtained through the replacement $\hat{t} \iff \hat{u}$. The function $f(k^2)$ representing the Standard Model Hgg triangle loop contribution, has been defined in (8) and in Appendix A1.

3 Sensitivity to NP couplings

3.1 From $\Gamma(H \rightarrow gg)$ measured at Linear Collider.

We give an estimate of the sensitivity to the NP couplings d_G and \tilde{d}_G for a light Higgs boson ($m_H \simeq 100 - 200 \text{ GeV}$), assuming a global uncertainty on $\Gamma(H \rightarrow gg)$ of about 40%. This would cover the theoretical uncertainties on α_s and higher QCD effects, as well as the experimental errors in the measurement of this decay width. It seems that even with a high energy, high luminosity e^+e^- Linear Collider (LC), this is the best one can expect [19]. With this assumption one obtains the sensitivity limits

$$|d_G| = \frac{v}{20}|f(0)| \quad , \quad |\tilde{d}_G|^2 = \frac{v^2}{40}|f(0)|^2 \quad (18)$$

which, using also the unitarity constraints (5, 6), means ³

$$|d_G| = 6. \times 10^{-4} \quad (\Lambda_{NP} = 36 \text{ TeV}) \quad , \quad |\tilde{d}_G| = 2. \times 10^{-3} \quad (\Lambda_{NP} = 20 \text{ TeV}) . \quad (19)$$

These would be already quite remarkable values. They arise because one compares tree level NP effects with 1-loop SM contributions.

3.2 From the Higgs production rate at LHC.

At LHC, Higgs production should be dominated by the $gg \rightarrow H$ process. We therefore consider the production rate in $pp \rightarrow H + X$ given by (11 - 14). Theoretically, the sensitivity to NP should be similar to the one expected from $\Gamma(H \rightarrow gg)$, as it is this

³Note that our notation for the NP scale is different from the one in [14].

same quantity which controls the production rate. Experimentally, this Higgs production process is very interesting, due to the large number of events expected in the various Higgs decay modes. For a light Higgs ($m_H \simeq 100 - 150$ GeV) the $\gamma\gamma$ channel is experimentally favored (since the statistics is enormous anyway), and the expected experimental accuracy is of a few percent [20].

In this analysis we assume that the NP effect on $Br(H \rightarrow \gamma\gamma)$ is negligible. This stems from the observation that it could only come from two possible sources. The first one is a direct NP effect on the $H\gamma\gamma$ coupling arising from other NP operators (not involving gluon fields), which can be constrained through different processes though, as discussed in [15, 16, 17, 9]. The second possible source comes from a modification of the $\Gamma(H \rightarrow gg)$ width induced by \mathcal{O}_{GG} , $\tilde{\mathcal{O}}_{GG}$, which in turn changes accordingly the total H -width and $Br(H \rightarrow \gamma\gamma)$. However, as the $Br(H \rightarrow gg)$ is only a few percent, even a 20% modification of $\Gamma(H \rightarrow gg)$, induces only a $\sim 1\%$ variation to $Br(H \rightarrow \gamma\gamma)$, which is negligible compared to the experimental uncertainty. In addition, to the already mentioned theoretical uncertainty in the QCD corrections, one should add the uncertainty in the parton (mainly the gluon) distribution functions. In [26, 34, 35], these are estimated to be of the order of $\pm 10\%$ to $\pm 20\%$. So they turn out to be the dominant source of uncertainty in this analysis. Assuming a global uncertainty of $\pm 20\%$ will give the sensitivities:

$$|d_G| \simeq 3. \times 10^{-4} \quad (51 \text{ TeV}) \quad , \quad |\tilde{d}_G| \simeq 1.4 \times 10^{-3} \quad (24 \text{ TeV}) \quad (20)$$

Numerically, these numbers are only slightly better than the ones given in the preceding Section on the basis of $\Gamma(H \rightarrow gg)$ at LC. But since LHC should anyway run before LC, we must emphasize the importance of these results, which give indeed very interesting constraints on the NP effects.

In concluding this subsection we note that the main difficulty here comes from theoretical uncertainties, which prohibit us to make a better benefit of the huge statistics brought in by LHC. This is why in the next Section, we turn to a theoretically cleaner NP signal, free of the normalization uncertainties of the total cross section.

3.3 From the shape of the H+jet distributions at LHC.

We now look at the NP signal based on the relative (but drastic) differences in the shape of the H production at large transverse momentum.

At $p_T \gtrsim m_t$, the SM distribution (based on the triangle Hgg and the box $Hggg$ contributions due to the top quark loop in Fig.1) starts being sensitive to the non-locality of the Hgg vertex and falls off; whereas the NP contribution (associated to a large scale Λ_{NP}) is still local and remains flat. In fact, one can check that the pure NP contribution behaves in the same way as the contribution called SM_{eff} in Figs.4-7 below, which is derived by taking the *large m_t limit* in SM and identifying $|d_G| = \frac{\alpha_s}{12\pi}$ or $|\tilde{d}_G| = \frac{\alpha_s}{12\pi}$, [22, 36].

The results for various ($H + jet$) distributions are shown in Figs.4-7. In all our illustrations $m_H = 100$ GeV is used, but we have checked that there is very little change

when this mass increases up to 200 GeV. In Figs.4-7, we compare the complete 1-loop SM prediction (labeled SM), with the large m_t approximation to SM (labeled SM_{eff}), and the effects due to the presence of the \mathcal{O}_{GG} operator with $d_G = +10^{-3}$ (labeled $+d_G$) or $d_G = -10^{-3}$ (labeled $-d_G$), as well as the effect of the $\tilde{\mathcal{O}}_{GG}$ contribution for $|\tilde{d}_G| = 10^{-3}$ (labeled \tilde{d}_G). The results include all possible subprocesses due to gg , gq , $g\bar{q}$ and $q\bar{q}$ initial states; compare (A.45-A.48). As shown in Fig.6, the subprocess $gg \rightarrow Hg$ dominates the p_T distribution for $x_T \equiv 2E_{TH}/\sqrt{s} \lesssim 0.1$; while for $x_T \gtrsim 0.1$ it is $gq, g\bar{q}$ that dominate; the $q\bar{q}$ contribution being always smaller.

The main features concerning the NP observability are discussed below:

Shape of y_H and χ distributions.

The shape of the y_H and χ (compare (A.42) distributions in Figs.4,5) do not seem to be notably different in the SM and in the NP cases. They only differ in absolute magnitude, roughly in the same way as the total production rate. So, from these measurements, we cannot expect an improvement in the determination of the NP couplings as compared to the one obtained from the total production rate.

Shape of x_T and M distributions.

On the contrary, the transverse energy and the $H + jet$ invariant mass distributions (Fig.6,7) are very sensitive to NP. At large x_T or M , the NP contributions differ from SM by a flattening of the distributions. As already stated, such behaviour is due to the locality of the NP interaction implied by its high Λ_{NP} scale. For the same reason, this is also true for the SM_{eff} approximation describing the large m_t limit of the SM, which should thus become inadequate for $p_T \gtrsim m_t$. The size of the NP effect, is fixed by the value of the d_G and \tilde{d}_G couplings, which once they are determined also fix the accessible values of Λ_{NP} through the unitarity relations (5, 6).

We also remark that the quadratic $\tilde{\mathcal{O}}_{GG}$ contribution always increases the rate, whereas the linear \mathcal{O}_{GG} one produces a constructive or destructive interference with SM, depending on the sign of d_G . The observation of a destructive effect would be a clear indication for \mathcal{O}_{GG} .

Ratios and sensitivity to NP

As already stated, this sensitivity is based on the change in the shape of the p_T distribution induced by NP. In order to quantify it, we consider the ratio

$$R = N_{High}/N_{Low} , \quad (21)$$

where N_{High} and N_{Low} are the number of ($H + jet$) events in the high and the low transverse energy domains $[x_i, x_{Tmax}]$ and $[x_{Tmin}, x_i]$, respectively; compare Fig.6. The lowest and highest points x_{Tmin}, x_{Tmax} are chosen as $x_{Tmin} = 0.0257$ and $x_{Tmax} = 0.25$; but the results are independent of their precise values. Note in particular that $x_{Tmin} = 0.0257$ corresponds to $p_T \simeq 150$ GeV, for which the use of the leading QCD expression should be adequate. The intermediate value x_i is chosen in order to maximize the sensitivity of

R to NP effects. It naturally turns out that x_i lies close to the value where the SM_{eff} prediction crosses the exact SM one. We choose therefore $x_i = 0.05$.

As seen in Fig.6, the number of events in the low x_T domain is determined solely by the SM contribution; while the NP effects mainly influence the events in the high x_T domain. This is even more pronounced for $x_T > 0.25$, but there are very few events there anyway. The NP observability limit is then defined by demanding that the NP effect on the ratio R is larger than the 1σ statistical fluctuations of it.

At LHC, with an integrated luminosity $L = 100 \text{ fb}^{-1}$ per year, and 3 years of running for the two experiments ATLAS and CMS, we find $N_{High}^{SM} = 22320$, $N_{Low}^{SM} = 417000$ at the two x_T domains. This should a priori lead to an excellent sensitivity to NP. However these numbers are reduced by the branching ratios of the Higgs boson to the observable channels and by detection efficiencies. For the mass range $100 \text{ GeV} \lesssim m_H \lesssim 200 \text{ GeV}$, the relevant subprocesses are $gg \rightarrow H \rightarrow \gamma\gamma$, $gg \rightarrow H \rightarrow WW^*$ and $gg \rightarrow H \rightarrow ZZ^*$ [20]. If we only use the $H \rightarrow \gamma\gamma$ mode, whose branching ratio is very low (about 2×10^{-3} for $m_H \lesssim 150 \text{ GeV}$ and negligible for higher masses), we obtain $N_{High}^{SM} = 22$, $N_{Low}^{SM} = 420$. With such numbers the statistical uncertainty on the ratio R is about 25%, which leads to sensitivity limits for the NP couplings similar to those given in (20).

This result can be substantially improved for most of the mass range $100 \text{ GeV} \lesssim m_H \lesssim 200 \text{ GeV}$, by using also the Higgs decay modes to WW^* , ZZ^* which strongly increase with m_H . Thus the WW^* (ZZ^*) modes reach *e.g.* at $m_H \sim 150 \text{ GeV}$ the level of 50% (5%) respectively. Above the corresponding thresholds, the WW and ZZ modes will of course dominate and greatly increase the statistics. In [20] an analysis of the two-weak boson final states is performed, which shows that their statistical error is already smaller than the one for the $\gamma\gamma$ case, in most of the above mass range. Considerable work should of course still be done on the detection of the various Higgs decay modes, before we fully identify all potentialities [20, 26]. Using though the existing results we are led to the conclusion that an improvement of the sensitivities given in (20) by a factor of 2 to 10, depending on m_H , should be possible. This is particularly true for $m_H \gtrsim 120 \text{ GeV}$.

We should also note that our present study of the p_T shape through the ratio R , is intended only as a preliminary orientation. In the actual search, a global study of the shape of the p_T spectrum should be done in a more precise way during the event selection, taking into account the p_T dependence of the background and all characteristics of the detectors⁴. This is beyond the scope of this paper and our competence. We nevertheless believe that our simple study has shown that it is reasonable to expect an appreciable improvement in the sensitivity to the NP contribution.

Finally we note that we obtain similar results by applying the same procedure to the invariant mass distribution. The intermediate value which optimizes the sensitivity is now found as $M_i \simeq 0.9 \text{ TeV}$. The results for d_G and \tilde{d}_G sensitivities turn out to be similar to the ones obtained from the x_T distribution.

⁴A recent study[37] of the process $pp \rightarrow \gamma\gamma + jet$ shows that the background has indeed different distributions.

4 Conclusion

In this paper we have studied the $dim = 6$ $SU(3) \times SU(2) \times U(1)$ gauge invariant operators \mathcal{O}_{GG} and $\tilde{\mathcal{O}}_{GG}$, which induce anomalous Higgs boson gluon interactions. Such effects should appear when the NP degrees of freedom carry colour and simultaneously couple to the Higgs sector. For studying the anomalous Hgg and $Hg\bar{g}$ couplings, we have looked at the tests which can be realized from Higgs production and decay.

At e^+e^- colliders, the measurement of the Hgg coupling has to rely on the difficult measurement of the $H \rightarrow gg$ width. At LEP2 only a few events could be observed. At a 500 GeV LC, for $m_H \simeq 100 - 150$ GeV, with a few hundreds of events accessible, one can only expect to reach the sensitivity limit

$$|d_G| \simeq 6. \times 10^{-4} \quad (\Lambda_{NP} \simeq 36 \text{ TeV}) \quad , \quad |\tilde{d}_G| \simeq 2. \times 10^{-3} \quad (\Lambda_{NP} \simeq 20 \text{ TeV}) \quad . \quad (22)$$

At LHC, the ggH coupling controls the H production rate. Statistics is huge. The main problem in this case is due to the large uncertainties (about 20%) in the QCD corrections to the total cross section. This limits the sensitivity to NP to the values:

$$|d_G| \simeq 3. \times 10^{-4} \quad (\Lambda_{NP} \simeq 36 \text{ TeV}) \quad , \quad |\tilde{d}_G| \simeq 1.4 \times 10^{-3} \quad (\Lambda_{NP} \simeq 20 \text{ TeV}) \quad , \quad (23)$$

for $100 \lesssim m_H \lesssim 200$ GeV. The importance of this LHC measurement, which in fact should precede the aforementioned one at a Linear Collider, should be appreciated.

The sensitivity to the NP couplings will be notably improved if at LHC we also study the shape of the $H + jet$ distributions at large transverse momentum or large invariant masses. The change which is induced in the shape of these distributions constitutes a clear signal for NP. We have explored this possibility by considering the ratio of the number of events at large transverse momentum or invariant mass to the one at low values. This quantity is rather insensitive to theoretical uncertainties (due to SM itself or to anomalous $g\bar{t}t$ or $H\bar{t}t$ couplings), but the precision is now controlled by the smallness of the expected statistics. If only the $H \rightarrow \gamma\gamma$ mode is used, we reach about the same sensitivity as the one given in (23). This is already a very interesting result as it constitutes a theoretically clean independent measurement. But now, depending of the value of the Higgs mass, the sensitivity can be notably improved by using the WW^* and ZZ^* modes, as well as the real WW and ZZ modes as soon as m_H goes above the corresponding thresholds. Depending on the value of the Higgs mass, we then expect an improvement by a factor 2 to 10 in these observability limits.

The values of the NP scales that such an analysis should allow to reach *i.e.* 50 to 100 TeV, are remarkable. They are of the same order of magnitude as the ones expected in the electroweak sector for the operators \mathcal{O}_{WW} , $\tilde{\mathcal{O}}_{WW}$, \mathcal{O}_{BB} and $\tilde{\mathcal{O}}_{BB}$ describing anomalous HZZ , $HZ\gamma$ and $H\gamma\gamma$ couplings and which affect the corresponding H decay modes as well as HZ , $H\gamma$ production in e^+e^- collisions and H production in $\gamma\gamma$ collisions, [9, 15, 16, 17].

A comparison of the effects or of the limits obtained in these two (electroweak and gluonic) sectors should tell us about the flavour and colour content of new physics.

Acknowledgments

We like to thank Abdelhak Djouadi and Michael Spira for enjoyable and useful discussions, and G. Tsirigoti for participating in the early stage of the present work.

Appendix A1: 1-loop SM contribution to the ggH amplitude

The form factor $\bar{f}(k^2)$ determining, (through the diagrams in Fig.1a), the Hgg coupling in SM in the case that the momentum k of one of the gluons may be off-shell, is

$$\bar{f}(k^2) = C_0(k^2) \left[1 - \frac{4m_t^2}{m_H^2 - k^2} \right] - \frac{2}{m_H^2 - k^2} + \frac{2k^2}{(m_H^2 - k^2)^2} F(k^2) , \quad (\text{A.1})$$

where all conventions are given in Sect.2.2. The triangle loop is computed through the FF-a package [38] using the standard Passarino-Veltman method [39] and the notations of [40] and [41] with

$$C_0(k^2) \equiv C_0(k^2, 0, m_H^2; m_t, m_t, m_t) . \quad (\text{A.2})$$

and

$$F(k^2) \equiv \int_0^1 dx \ln \frac{[(1-x)m_1^2 + xm_2^2 - x(1-x)m_H^2 - i\epsilon]}{[(1-x)m_1^2 + xm_2^2 - x(1-x)k^2 - i\epsilon]} \quad (\text{A.3})$$

In the limit $k^2 \rightarrow 0$, in which both gluons are on-shell, $\bar{f}(0)$ matches the result [23, 28, 29]

$$\bar{f}(0) = -\frac{\tau_t}{2m_t^2} (1 + (1 - \tau_t) \tilde{f}(\tau_t)) , \quad (\text{A.4})$$

where $\tau_t = 4m_t^2/m_H^2$ and

$$\begin{aligned} \tilde{f}(\tau_t) &= [\sin^{-1}(1/\sqrt{\tau_t})]^2 && \text{if } \tau_t \geq 1 , \\ \tilde{f}(\tau_t) &= -\frac{1}{4} \left[\ln \left(\frac{1 + \sqrt{1 - \tau_t}}{1 - \sqrt{1 - \tau_t}} \right) - i\pi \right]^2 && \text{if } \tau_t < 1 . \end{aligned} \quad (\text{A.5})$$

Appendix A2 : CP conserving amplitudes for $gg \rightarrow Hg$

Below we discuss the 1-loop SM contribution, as well as the CP conserving NP contribution, to the invariant amplitudes for the process

$$g(\epsilon, k, a) + g(\epsilon', k', b) \rightarrow H(q) + g(e, q', c) , \quad (\text{A.6})$$

where the polarization, momenta and colour indices of the gluons are indicated in parentheses. The 1-loop SM contribution to this amplitude has been computed long ago by R.K. Ellis *et.al.* [29]. It arises from the triangle and box terms appearing in Fig.1 and involved in Fig.3. We have recomputed their result in order to make sure that the NP contribution is added correctly to the SM one.

If Bose-symmetry among the three external gluons were ignored, there would have been 14 different Lorentz invariant and CP conserving forms contributing to the amplitude,

which are reduced to just 4 ones, when gauge symmetry is imposed. For the gluon momenta and polarizations indicated in (A.6), these are

$$N_1 = [(e.k)(k'.q') - (e.k')(k.q')] \{ (k.q')[(\epsilon.\epsilon')(k'.q') - (\epsilon.k')(\epsilon'.q')] \\ + (\epsilon'.q')(\epsilon.q')(k.k') - (\epsilon.q')(\epsilon'.k)(q'.k') \} , \quad (\text{A.7})$$

$$N_2 = [(\epsilon.e)(k.q') - (\epsilon.q')(e.k)][(\epsilon'.k)(k'.q') - (\epsilon'.q')(k.k')] , \quad (\text{A.8})$$

$$N_3 = [(\epsilon'.e)(k'.q') - (\epsilon'.q')(e.k')][(\epsilon.k')(k.q') - (\epsilon.q')(k.k')] , \quad (\text{A.9})$$

$$N_4 = [(e.k)(k'.q') - (e.k')(q'.k)][(\epsilon.k')(k.q') - (\epsilon.q')(k.k')] \cdot \\ [(\epsilon'.k)(k'.q') - (\epsilon'.q')(k.k')] . \quad (\text{A.10})$$

As a result the total contribution to the amplitude is written as⁵

$$R(gg \rightarrow Hg) = -f_{abc} \sum_{j=1}^4 A_j(\hat{s}, \hat{t}, \hat{u}) N_j , \quad (\text{A.11})$$

where

$$\hat{s} = (k+k')^2, \quad \hat{t} = (q-k)^2, \quad \hat{u} = (q'-k)^2 , \quad (\text{A.12})$$

with the momenta defined in (A.6). The A_j amplitudes in (A.11) are not the same as the ones used in [29]. In accordance with this reference, the requirements of Bose-Einstein statistics among the three external gluons reduce the number of these amplitudes to two, by determining A_2 , A_3 in terms of A_1 , through

$$A_2(\hat{s}, \hat{t}, \hat{u}) = \frac{\hat{t}\hat{s}}{2\hat{u}} A_1(\hat{u}, \hat{t}, \hat{s}) , \quad (\text{A.13})$$

$$A_3(\hat{s}, \hat{t}, \hat{u}) = -\frac{\hat{u}\hat{s}}{2\hat{t}} A_1(\hat{t}, \hat{s}, \hat{u}) , \quad (\text{A.14})$$

and imposing the constraints

$$A_1(\hat{s}, \hat{t}, \hat{u}) = A_1(\hat{s}, \hat{u}, \hat{t}) , \quad (\text{A.15})$$

$$A_4(\hat{s}, \hat{t}, \hat{u}) = A_4(\hat{s}, \hat{u}, \hat{t}) , \quad (\text{A.16})$$

$$A_4(\hat{s}, \hat{t}, \hat{u}) - A_4(\hat{t}, \hat{s}, \hat{u}) = \frac{2}{\hat{t}} A_1(\hat{t}, \hat{s}, \hat{u}) - \frac{2}{\hat{s}} A_1(\hat{s}, \hat{t}, \hat{u}) . \quad (\text{A.17})$$

Thus, we only need to give the 1-loop SM and the tree level \mathcal{O}_{GG} contributions to A_1 and A_4 , which are

$$A_1(\hat{s}, \hat{t}, \hat{u}) = \frac{2g_s^3 m_t^2}{\pi^2 v \hat{t} \hat{u}^2} \left[\frac{\hat{t} - m_H^2}{\hat{t}} \bar{f}(\hat{t}) - \frac{\hat{u}}{\hat{s}} \bar{f}(\hat{s}) + \frac{1}{2} \bar{b}_1 \right] + \left(\frac{32g_s d_G}{v} \right) \frac{(\hat{u} + \hat{s})(\hat{t} + \hat{s})}{\hat{s} \hat{t}^2 \hat{u}^2} , \quad (\text{A.18})$$

⁵The R amplitude has the phase of the S -matrix elements. We use the same conventions for the couplings as in [1, 42].

$$A_4(\hat{s}, \hat{t}, \hat{u}) = \frac{2g_s^3 m_t^2}{\pi^2 v \hat{t} \hat{u}^2} \left[\frac{2}{\hat{t}} f(\hat{t}) + \frac{1}{2} \bar{b}_8 \right] - \frac{64 g_s d_G}{v \hat{t}^2 \hat{u}^2}, \quad (\text{A.19})$$

where \bar{b}_1 and \bar{b}_8 , in (A.18, A.19) arise from the SM box diagram in Fig.1b. They are expressed in terms of the D functions defined in [40] and [41] as⁶

$$D_i = D_i(0, 0, 0, m_H^2, \hat{u}, \hat{s}; m_t, m_t, m_t, m_t), \quad (\text{A.20})$$

$$\overline{D}_i = D_i(0, 0, 0, m_H^2, \hat{u}, \hat{t}; m_t, m_t, m_t, m_t), \quad (\text{A.21})$$

$$\overline{\overline{D}}_i = D_i(0, 0, 0, m_H^2, \hat{t}, \hat{s}; m_t, m_t, m_t, m_t). \quad (\text{A.22})$$

$$\begin{aligned} \bar{b}_1 = & m_t^2 (D_0 + 2D_{13} - 2\overline{\overline{D}}_{12} + \overline{D}_0) \\ & + \hat{t} (-2D_{133} + 2\overline{\overline{D}}_{122} - D_{25} - 2D_{23} - \overline{D}_{26} + 2\overline{\overline{D}}_{22} + 2\overline{\overline{D}}_{24} - D_{13} + 2\overline{\overline{D}}_{12}) \\ & + \hat{u} (-2D_{123} + 2\overline{\overline{D}}_{123} - D_{24} - 2D_{26} - 2D_{25} - \overline{D}_{24} + 2\overline{\overline{D}}_{26} \\ & - \frac{1}{2}D_0 - D_{12} - 2D_{13} - \frac{1}{2}\overline{D}_0 - \overline{D}_{12} - \frac{1}{2}\overline{\overline{D}}_0) \\ & + \hat{s} (-2D_{233} + 2\overline{\overline{D}}_{223} - D_{26} - 2D_{23} - \overline{D}_{25} + 2\overline{\overline{D}}_{26} - D_{13} + \overline{\overline{D}}_{12}) \\ & - 4D_{003} - 8\overline{D}_{003} + 4\overline{\overline{D}}_{002} - 4D_{27} - 4\overline{D}_{27} + 4\overline{\overline{D}}_{27}, \end{aligned} \quad (\text{A.23})$$

$$\bar{b}_8 = 8(D_{233} - \overline{D}_{133} - \overline{\overline{D}}_{223} + D_{23} - \overline{D}_{23} - \overline{\overline{D}}_{26}) + 2(D_{13} - \overline{D}_{13} - \overline{\overline{D}}_{12}). \quad (\text{A.24})$$

and computed using the FF-package [38].

We have checked (numerically) that all gauge non-invariant terms arising from the individual diagrams in Fig.3, cancel out when they are added. A further test is provided by the various Bose statistics relations (A.15-A.17) and (A.13, A.14), which are also perfectly satisfied.

Appendix A3 : Kinematics for H+jet production in the parton model

The basic parton model expression for the hadron-hadron collision $AB \rightarrow Hf\dots$, taking place through the subprocesses $a + b \rightarrow H + f$ and illustrated in Fig.2, is written as [42]

$$\sigma(AB \rightarrow H f \dots) = \sum_{ab} \int \int dx_a dx_b f_{a/A}(x_a) f_{b/B}(x_b) \hat{\sigma}(ab \rightarrow Hf), \quad (\text{A.25})$$

with f being a gluon or massless quark jet. Here $f_{a/A}(x_a)$ is the distribution function of partons of type ($a = g, q, \bar{q}$), in the hadron of type A .

⁶See in particular Eqs.(D.12) of [40].

We next list a few formulae for the kinematics. The transverse momenta of the produced H and the f -jet $p_T \equiv p_{TH} = p_{Tf}$ and the energy $E_{HT} = \sqrt{p_T^2 + m_H^2}$ are described through

$$x_T = \frac{2E_{HT}}{\sqrt{s}}, \quad \beta_T = p_T/E_{TH} = \sqrt{1 - \frac{4m_H^2}{sx_T^2}}, \quad x_{fT} = \frac{2E_{fT}}{\sqrt{s}} = \beta_T x_T. \quad (\text{A.26})$$

The rapidities of the Higgs and the outgoing jet f , in the laboratory system are related to their energies and momenta along the beam-axis of hadron A , (taken as the \hat{z} -axis) and to the corresponding production angles by

$$e^{2y_H} = \frac{E_H + p_H \cos \theta_H}{E_H - p_H \cos \theta_H}, \quad (\text{A.27})$$

$$e^{2y_f} = \frac{E_f + p_f \cos \theta_f}{E_f - p_f \cos \theta_f}. \quad (\text{A.28})$$

The center-of-mass rapidity \bar{y} of the Hf pair, and the rapidities y_H^* , y_f^* in c.m., are defined as

$$y_H = \bar{y} + y_H^*, \quad y_f = \bar{y} + y_f^*. \quad (\text{A.29})$$

The fractions of momenta carried by the incoming partons are given by

$$x_a = \frac{x_T}{2} [e^{y_H} + \beta_T e^{y_f}] = \frac{M}{\sqrt{s}} e^{\bar{y}}, \quad (\text{A.30})$$

$$x_b = \frac{x_T}{2} [e^{-y_H} + \beta_T e^{-y_f}] = \frac{M}{\sqrt{s}} e^{-\bar{y}}, \quad (\text{A.31})$$

while the Mandelstam invariants of the subprocesses satisfy

$$\hat{s} \equiv M^2 = (p_a + p_b)^2 = x_a x_b s = E_{TH}^2 [1 + \beta_T^2 + 2\beta_T \cosh(\Delta y)], \quad (\text{A.32})$$

$$\hat{t} = (p_H - p_a)^2 = -E_{TH}^2 \beta_T (\beta_T + e^{-\Delta y}), \quad (\text{A.33})$$

$$\hat{u} = (p_f - p_a)^2 = -E_{TH}^2 \beta_T (\beta_T + e^{\Delta y}), \quad (\text{A.34})$$

$$\tau = \frac{\hat{s}}{s} = x_a x_b, \quad (\text{A.35})$$

where

$$\Delta y \equiv y_H - y_f = y_H^* - y_f^*. \quad (\text{A.36})$$

Denoting the c.m. *Higgs* particle production angle by θ^* and the c.m. H velocity by

$$\beta = p_H^*/E_H^* = \frac{\hat{s} - m_H^2}{\hat{s} + m_H^2}, \quad (\text{A.37})$$

we have also the expressions

$$M = E_{TH}(1 + \beta) \cosh y_H^* = p_T \left(\frac{1}{\beta} + 1 \right) \cosh y_f^* , \quad (\text{A.38})$$

$$\hat{t} = \frac{(m_H^2 - \hat{s})}{2} (1 - \cos \theta^*) , \quad (\text{A.39})$$

$$\hat{u} = \frac{(m_H^2 - \hat{s})}{2} (1 + \cos \theta^*) , \quad (\text{A.40})$$

$$\cos \theta^* = \frac{\tanh y_H^*}{\beta} = -\tanh y_f^* , \quad (\text{A.41})$$

$$\chi \equiv e^{2y_H^*} = \frac{\hat{u} - m_H^2}{\hat{t} - m_H^2} = \frac{1 + \beta \cos \theta^*}{1 - \beta \cos \theta^*} . \quad (\text{A.42})$$

The basic triple distribution is obtained from (A.25) to be

$$\frac{d\sigma}{dp_T^2 dy_H dy_f} = \tau S_{ij} \quad (\text{A.43})$$

where, according to (A.25), S_{ij} is the total probability

$$S_{ij} \equiv S_{gg} + S_{gq} + S_{g\bar{q}} + S_{q\bar{q}} \quad (\text{A.44})$$

with

$$S_{gg} \equiv g(x_a)g(x_b) \frac{d\hat{\sigma}(gg \rightarrow Hg)}{d\hat{t}} , \quad (\text{A.45})$$

$$S_{gq} \equiv \sum_q \left[g(x_a)q(x_b) \frac{d\hat{\sigma}(gq \rightarrow Hq)}{d\hat{t}} + q(x_a)g(x_b) \frac{d\hat{\sigma}(qg \rightarrow Hq)}{d\hat{t}} \right] , \quad (\text{A.46})$$

$$S_{g\bar{q}} \equiv \sum_{\bar{q}} \left[g(x_a)\bar{q}(x_b) \frac{d\hat{\sigma}(g\bar{q} \rightarrow H\bar{q})}{d\hat{t}} + \bar{q}(x_a)g(x_b) \frac{d\hat{\sigma}(\bar{q}g \rightarrow H\bar{q})}{d\hat{t}} \right] , \quad (\text{A.47})$$

$$S_{q\bar{q}} \equiv \sum_q \left[q(x_a)\bar{q}(x_b) \frac{d\hat{\sigma}(q\bar{q} \rightarrow Hg)}{d\hat{t}} + \bar{q}(x_a)q(x_b) \frac{d\hat{\sigma}(\bar{q}q \rightarrow Hg)}{d\hat{t}} \right] . \quad (\text{A.48})$$

where $q = u, d, s, c, b$. From this basic distribution and imposing the cuts

$$|y_H| \leq Y_H, \quad |y_f| \leq Y_f , \quad (\text{A.49})$$

we get:

The transverse energy distribution

$$\frac{d\sigma}{dx_T} = \int dy_H \int dy_f \frac{M^2 x_T}{2} S_{ij} , \quad (\text{A.50})$$

where M^2 is determined from (A.32) and the integration limits are

$$\begin{aligned} y_{f\min} &= \max \left\{ \ln \left(\frac{\beta_T x_T}{2 - x_T e^{-y_H}} \right); -Y_f \right\}, \\ y_{f\max} &= \min \left\{ \ln \left(\frac{2 - x_T e^{y_H}}{\beta_T x_T} \right); Y_f \right\}, \end{aligned} \quad (\text{A.51})$$

$$\begin{aligned} y_{H\max} = -y_{H\min} &= \\ \min \left\{ Y_H; \ln \left(\frac{2}{x_T} \right); \cosh^{-1} \left(\frac{1}{x_T} \left(1 + \frac{m_H^2}{s} \right) \right); \ln \left(\frac{2 - \beta_T x_T e^{-Y_f}}{x_T} \right) \right\}. \end{aligned} \quad (\text{A.52})$$

The rapidity distribution

Since this is symmetric in y_H , we may consider

$$\frac{d\sigma}{d|y_H|} = \int dx_T \int dy_f M^2 x_T S_{ij}, \quad (\text{A.53})$$

where the y_f -limits are given (A.51), while the limits of the x_T integration are

$$\begin{aligned} x_{T\min} &= x_{T\min, \text{exp}} > \frac{2m_H}{\sqrt{s}}, \\ x_{T\max} &= \min \left\{ \frac{1 + \frac{m_H^2}{s}}{\cosh y_H}; \frac{2e^{2Y_f \pm y_H} - \sqrt{\Delta_1}}{e^{2(Y_f \pm y_H)} - 1}; 2e^{\pm y_H} \right\} \end{aligned} \quad (\text{A.54})$$

with

$$\Delta_1 = 4[e^{2Y_f} + \frac{m_H^2}{s}(1 - e^{2(Y_f - y_H)})]. \quad (\text{A.55})$$

The invariant mass distribution

Using the c.m. rapidity \bar{y} defined above and (A.42), one obtains

$$\frac{d\sigma}{dM^2} = \int d\chi \int d\bar{y} \frac{(M^2 + m_H^2)}{s(1 + \chi)^2} S_{ij}, \quad (\text{A.56})$$

where the integration limits are

$$\begin{aligned} \bar{y}_{\max} &= \min \left\{ Y_H - \frac{1}{2} \ln \chi; Y_f - \frac{1}{2} \ln \left(\frac{M^2 - \chi m_H^2}{M^2 \chi - m_H^2} \right); \ln \left(\frac{\sqrt{s}}{M} \right) \right\}, \\ \bar{y}_{\min} &= \max \left\{ -Y_H - \frac{1}{2} \ln \chi; -Y_f - \frac{1}{2} \ln \left(\frac{M^2 - \chi m_H^2}{M^2 \chi - m_H^2} \right); -\ln \left(\frac{\sqrt{s}}{M} \right) \right\}, \end{aligned} \quad (\text{A.57})$$

$$\begin{aligned} \chi_{\max} &= \min \left\{ \frac{M^2}{m_H^2}; \frac{M^2(s + m_H^2 e^{-2Y_f})}{M^4 e^{-2Y_f} + s m_H^2}; \frac{m_H^2(1 - e^{2(Y_H + Y_f)}) + \sqrt{\Delta_2}}{2M^2}; \frac{s}{M^2} e^{2Y_H} \right\}, \\ \chi_{\min} &= \max \left\{ \frac{m_H^2}{M^2}; \frac{M^4 e^{-2Y_f} + s m_H^2}{M^2(s + m_H^2 e^{-2Y_f})}; \frac{2M^2}{m_H^2(1 - e^{2(Y_H + Y_f)}) + \sqrt{\Delta_2}}; \frac{M^2}{s} e^{-2Y_H} \right\} \end{aligned} \quad (\text{A.58})$$

where

$$\Delta_2 = m_H^4 (e^{2(Y_H+Y_f)} - 1)^2 + 4M^4 e^{2(Y_H+Y_f)}. \quad (\text{A.59})$$

The angular distribution is given by

$$\frac{d\sigma}{d\chi} = \int dM^2 \int d\bar{y} \frac{(M^2 + m_H^2)}{s(1 + \chi)^2} S_{ij}. \quad (\text{A.60})$$

The \bar{y} integration limits are as in (A.57), while for the M^2 integration we have the limits

$$\begin{aligned} M_{max}^2 &= \min \left\{ \chi s e^{2Y_H}; \frac{s}{\chi} e^{2Y_H}; M_+^2; M_+'^2; s \right\}, \\ M_{min}^2 &= \max \left\{ \frac{\chi m_H^2 (e^{2(Y_f+Y_H)} - 1)}{\chi^2 e^{2(Y_f+Y_H)} - 1}; \frac{\chi m_H^2 (e^{2(Y_f+Y_H)} - 1)}{e^{2(Y_f+Y_H)} - \chi^2}; M_-^2; M_-'^2 \right\}, \end{aligned} \quad (\text{A.61})$$

where

$$M_{\pm}^2 = \frac{1}{2} [\chi(m_H^2 + s e^{2Y_f}) \pm \sqrt{\Delta_3}], \quad (\text{A.62})$$

$$\Delta_3 = \chi^2 (m_H^2 + s e^{2Y_f})^2 - 4s m_H^2 e^{2Y_f}, \quad (\text{A.63})$$

$$M_{\pm}'^2 = \frac{1}{2\chi} [m_H^2 + s e^{2Y_f} \pm \sqrt{\Delta_3'}], \quad (\text{A.64})$$

$$\Delta_3' = (m_H^2 + s e^{2Y_f})^2 - 4s m_H^2 \chi^2 e^{2Y_f}. \quad (\text{A.65})$$

References

- [1] J.F. Gunion, H.E. Haber, G.L. Kane and S. Dawson, "The Higgs Hunter Guide", Addison-Wesley, Reading MA, 1990.
- [2] W. Murray, talk presented at HEP 97, Jerusalem (1997).
- [3] The LEP Collaborations, the LEP Electroweak Working Group and the SLD Heavy Flavour Group, CERN-PPE/97-154 (1997).
- [4] G. Altarelli, R. Barbieri and F. Caravaglios, CERN-TH-97-290, hep-ph/9712368 (1997).
- [5] W. Buchmüller and D. Wyler, Nucl. Phys. **B268** (1986) 621; C.J.C. Burgess and H.J. Schnitzer, Nucl. Phys. **B228** (1983) 454; C.N. Leung, S.T. Love and S. Rao Z. f. Phys. **C31** (1986) 433; C. Arzt, M.B. Einhorn and J. Wudka, Nucl. Phys. **B433** (1995) 41.
- [6] G.J. Gounaris, D.T. Papadamou and F.M. Renard, Z. f. Phys. **C76** (1997) 333, hep-ph/9609437.
- [7] K. Whisnant, J.M. Yang, B.-L. Young and X. Zhang, Phys. Rev. **D56** (1997) 467, hep-ph/9702305.
- [8] K. J.M. Yang and B.-L. Young, Phys. Rev. **D56** (1997) 5907, hep-ph/9703463
- [9] G.J. Gounaris and G. Tsirigoti, Phys. Rev. **D56** (1997) 3030.
- [10] G. Altarelli, R. Barbieri and F. Caravaglios Phys. Lett. **B314** (1993) 357; K. Hagiwara et al, Phys. Lett. **B283** (1992) 353; Phys. Rev. **D48** (1993) 2182; A. De Rújula *et.al.*, Nucl. Phys. **B384** (1992) 3; G. Gounaris, F.M. Renard and C. Verzegnassi, Phys. Rev. **D52** (1995) 451.
- [11] Physics at LEP2, Yellow Report CERN 96-01, vol.1,2 edited by G. Altarelli, T. Sjöstrand and F. Zwirner.
- [12] Proc. on the Workshop on e^+e^- Collisions at TeV Energies: The Physics Potential edited by P.M. Zerwas, DESY 92-123A,B, 93-123C, 96-123D; E. Accomando *et.al.*, DESY 97-10, hep-ph/9705442, to appear in Phys. Reports; G.J. Gounaris, M. Kuroda and F.M. Renard, Phys. Rev. **D54** (1996) 6861.
- [13] E.H. Simmons Phys. Lett. **B226** (1989) 132; Phys. Lett. **B246** (1990) 471; P. Cho and E.H. Simmons, Phys. Lett. **B323** (1994) 401; H. Dreiner, A. Duff and D. Zeppenfeld, Phys. Lett. **B282** (1992) 441; G.J. Gounaris, D.T. Papadamou and F.M. Renard, hep-ph/9711399, to appear in Phys. Rev. D.
- [14] Uma Mahanta, MRI-PHY-971217, hep-ph/9712373 (1997).

- [15] K. Hagiwara, R. Szalapski and D. Zeppenfeld, Phys. Lett. **B318** (1993) 155; V. Barger, F.Cheung, A. Djouadi, B.A. Kniehl and P.M. Zerwas, Phys. Rev. **D49** (1994) 79; M. Krämer, J. Kühn, M.L. Stong and P.M. Zerwas, Z. f. Phys. **C64** (1994) 21. K. Hagiwara and M.L. Stong Z. f. Phys. **C92** (1994) 99.
- [16] G.J. Gounaris, F.M. Renard and N.D. Vlachos, Nucl. Phys. **B459** (1996) 51.
- [17] S.Y. Choi and K. Hagiwara, Phys. Lett. **B359** (1995) 369; G.J. Gounaris and F.M. Renard, Z. f. Phys. **C69** (1996) 513; G.J. Gounaris, J. Layssac and F.M. Renard, Z. f. Phys. **C65** (1995) 254, Z. f. Phys. **C67** (1995) 542.
- [18] J.L. Diaz-Cruz, M.A. Perez and J.J. Toscano, Phys. Lett. **B398** (1997) 347.
- [19] M.D. Hildreth, T. L. Barklow and D. L. Burke, Phys. Rev. **D49** (1994) 3441.
- [20] J.F. Gunion et al, Proc. 1996 DPF/DFB Summer study on "New Directions in High Energy Physics" (Snowmass 1996), hep-ph/9703330; J.F. Gunion, hep-ph/9705282, to appear in *Perspectives in Higgs Physics.* , ed. G. Kane, 2nd edition (World Scientific Publishing); Atlas Technical Proposal, CERN/LHCC 94-43(1994); CMS Technical Proposal, CERN/LHCC 94-38(1994).
- [21] A. Djouadi, M. Spira and P.M. Zerwas, Phys. Lett. **B264** (1991) 440.
- [22] S. Dawson, Nucl. Phys. **B359** (1991) 283.
- [23] J. Ellis, M.K. Gaillard and D.V. Nanopoulos, Nucl. Phys. **B106** (1976) 292; F. Wilczek, Phys. Rev. Lett. **39** (1977) 1304; A.I. Vainshtein, M.B. Voloshin, V.I. Sakharov and M.A. Shifman, Sov. J. Nucl. Phys. **30**(1979)711; J. Ellis, M.K. Gaillard and D.V. Nanopoulos and S.T. Sachrajda, Phys. Lett. **83B** (1979) 339; T.G. Rizzo, Phys. Rev. **D22** (1980) 178.
- [24] M. Spira, A. Djouadi, D. Graudens and P.M. Zerwas, Nucl. Phys. **B453** (1995) 17.
- [25] M. Spira and P.M. Zerwas, Lectures at Internatonale Unversitätswochen für Kern- und Teilchenphysik, Schladming 1997, hep-ph/9803257;
- [26] M. Spira, hep-ph/9705337.
- [27] M. Krämer, E. Laenen and M. Spira, Nucl. Phys. **B511** (1998) 523.
- [28] I. Hinchliffe and S.F. Novaes, Phys. Rev. **D38** (1988) 3475; R.P. Kauffman, Phys. Rev. **D44** (1991) 1415.
- [29] R.K. Ellis, I. Hinchliffe, M.Soldate and J.J. van der Bij, Nucl. Phys. **B297** (1988) 221.
- [30] G.J. Gounaris, J. Layssac and F.M. Renard, Phys. Lett. **B332** (1994) 146; G.J. Gounaris, J. Layssac, J.E. Paschalis and F.M. Renard, Z. f. Phys. **C66** (1995) 619; G.J. Gounaris, F.M. Renard and G. Tsirigoti, Phys. Lett. **B350** (1995) 212.

- [31] H.M. Georgi, S.L. Glashow, M.E. Machasek and D.V. Nanopoulos, *Phys. Rev. Lett.* **40** (1978) 692.
- [32] D. Graudenz, M. Spira, and P.M. Zerwas, *Phys. Rev. Lett.* **70** (1993) 1372.
- [33] M. Spira, A. Djouadi, D. Graudenz and P.M. Zerwas, *Phys. Lett.* **B318** (1993) 347.
- [34] Z. Kunszt, S. Moretti and W.J. Stirling, *Z. f. Phys.* **C74** (1997) 479.
- [35] A.D. Martin, R.G. Roberts, W.J. Stirling and R.S. Thorne, [hep-ph/9803445](#).
- [36] S. Dawson, [hep-ph/9703387](#).
- [37] S. Abdullin et al, preprint INP MSU 98-13/514, [hep-ph/9805341](#).
- [38] G.J. van Oldenborgh, FF-a package to evaluate one-loop Feynman diagrams, *Comp.Phys.Comm.* **66**(1991)1.
- [39] G. Passarino and M. Veltman, *Nucl. Phys.* **B160** (1979) 151.
- [40] K. Hagiwara, S. Matsumoto, D. Haidt and C.S. Kim, *Z. f. Phys.* **C64** (1995) 559.
- [41] Rolf Mertig, *Guide to FeynCalc* (1992)
- [42] R.K. Ellis, W.J. Stirling and B.R. Webber, *QCD and Collider Physics*, Cambridge Univ. Press 1996, Cambridge, UK.

Figure captions

Fig.1 Diagrams for top quark loop SM contributions to Hgg and $Hggg$ couplings.

Fig.2 Diagrams for $p + p \rightarrow H + jet + X$.

Fig.3 Diagrams for $gg \rightarrow Hg$, $gq \rightarrow Hq$ and $q\bar{q} \rightarrow Hg$.

Fig.4 Rapidity distribution in $p + p \rightarrow H + jet + X$ at LHC, for $m_H = 100$ GeV. SM describes 1-loop SM predictions; SM_{eff} the large m_t approximation to SM; $+d_G$ and $-d_G$ describe the \mathcal{O}_{GG} contributions for $d_G = +10^{-3}$ and $d_G = -10^{-3}$ respectively; and \tilde{d}_G describes the $\tilde{\mathcal{O}}_{GG}$ contribution for $|d_G| = 10^{-3}$.

Fig.5 Angular distribution in $p + p \rightarrow H + jet + X$ at LHC. See caption of Fig.4.

Fig.6 Transverse energy distribution in $p + p \rightarrow H + jet + X$ at LHC. See caption of Fig.4.

Fig.7 Invariant mass distribution in $p + p \rightarrow H + jet + X$ at LHC. See caption of Fig.4.

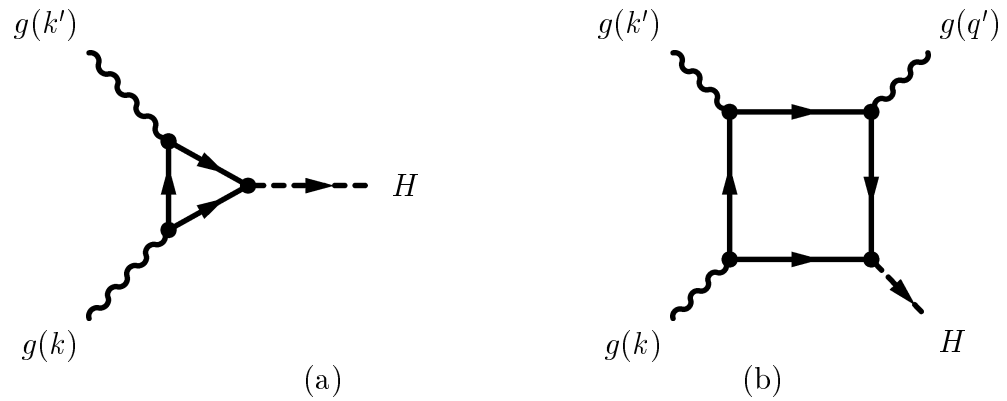


Fig. 1

Diagrams for top quark loop SM contributions to Hgg and $Hggg$ couplings.

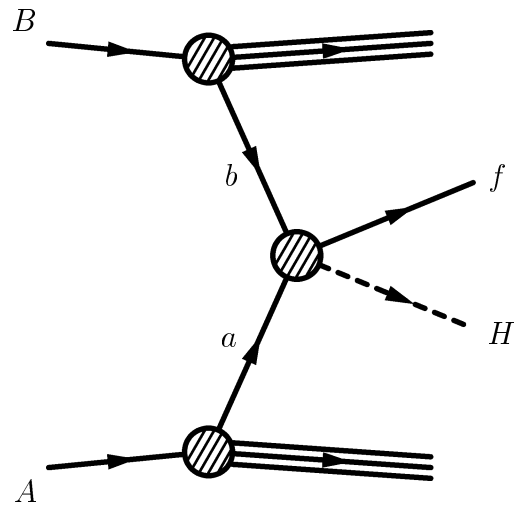
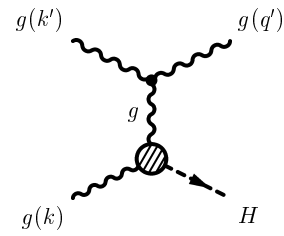
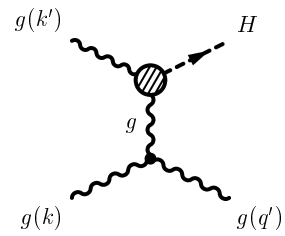


Fig. 2

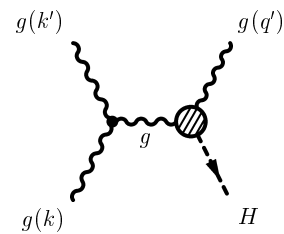
Diagrams for $p + p \rightarrow H + \text{jet} + X$.



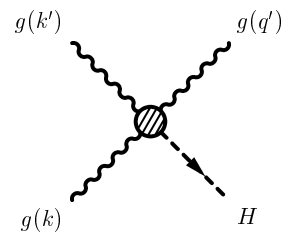
(a)



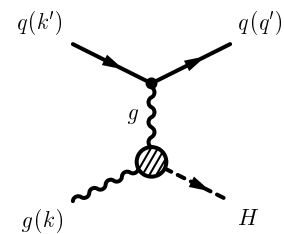
(b)



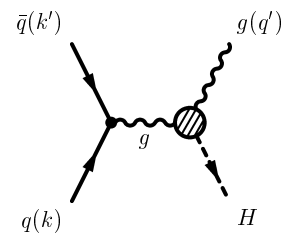
(c)



(d)



(e)



(f)

Fig. 3

Diagrams for $gg \rightarrow Hg$, $gq \rightarrow Hq$ and $q\bar{q} \rightarrow Hg$.

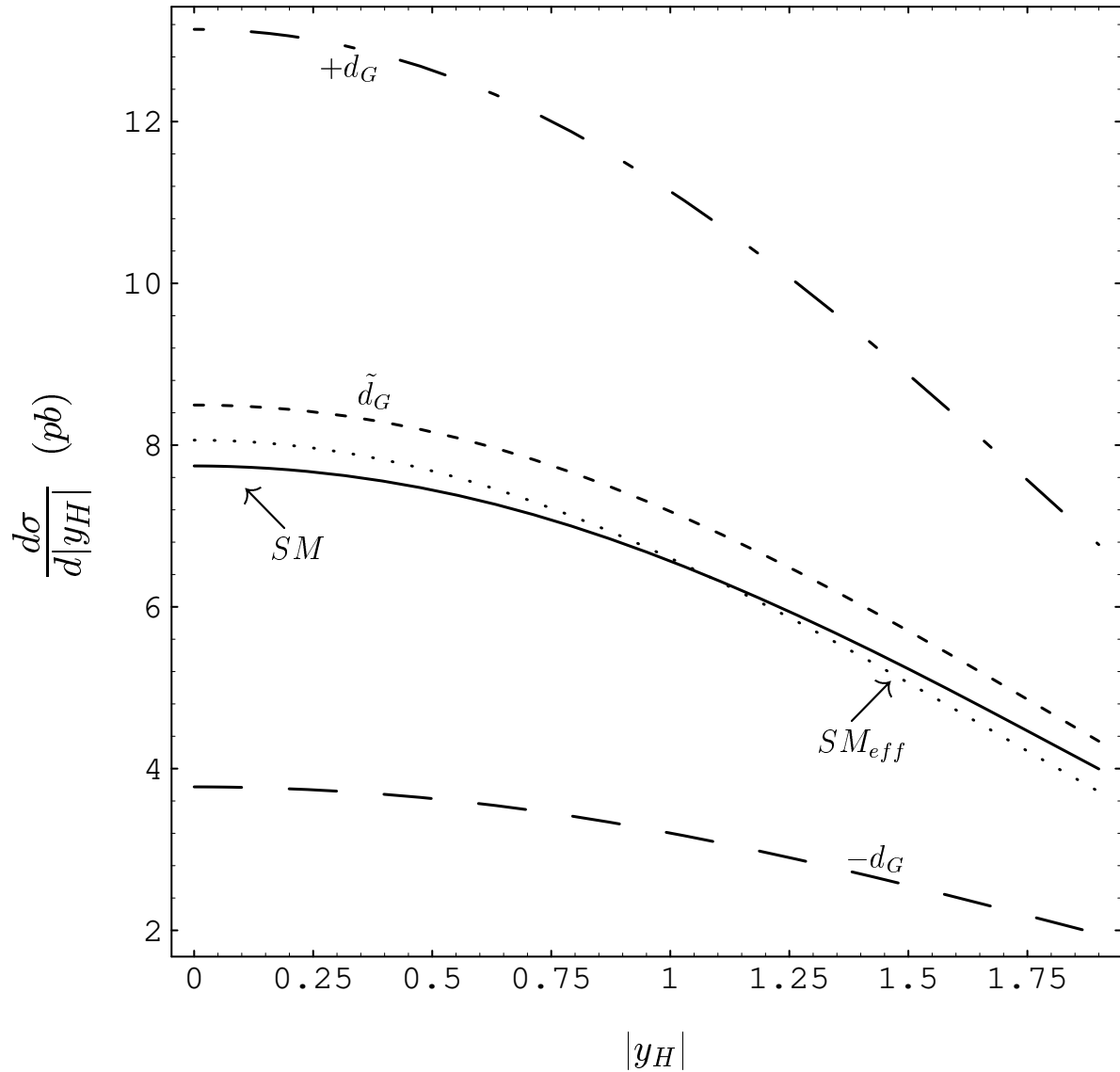


Fig. 4

Rapidity distribution in $p + p \rightarrow H + \text{jet} + X$ at LHC, for $m_H = 100 \text{ GeV}$. SM describes 1-loop SM predictions; SM_{eff} the large m_t approximation to SM; $+d_G$ and $-d_G$ describe the \mathcal{O}_{GG} contributions for $d_G = +10^{-3}$ and $d_G = -10^{-3}$ respectively; and \tilde{d}_G describes the $\tilde{\mathcal{O}}_{GG}$ contribution for $|\tilde{d}_G| = 10^{-3}$.

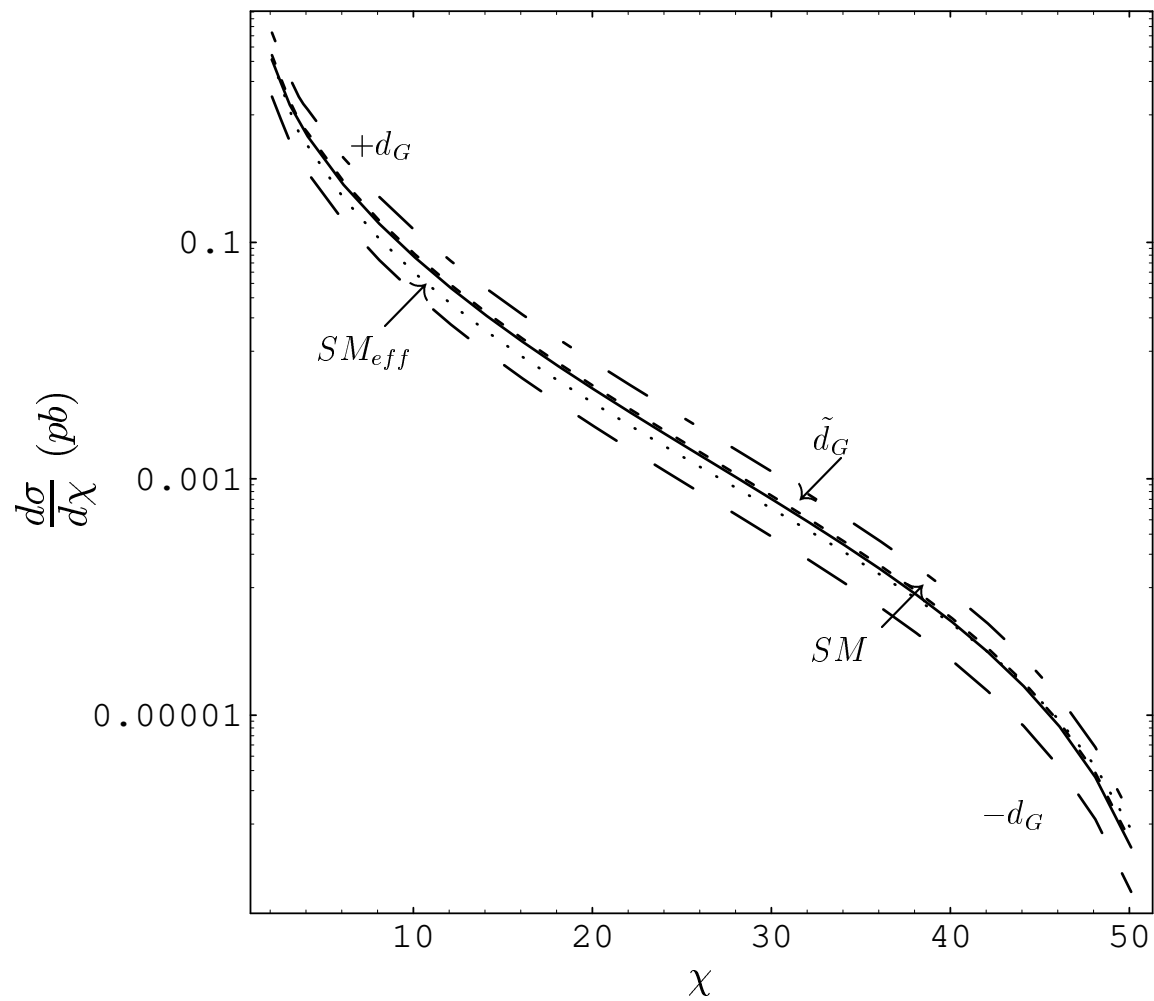


Fig. 5

Angular distribution in $p + p \rightarrow H + \text{jet} + X$ at LHC. See caption of Fig.4.

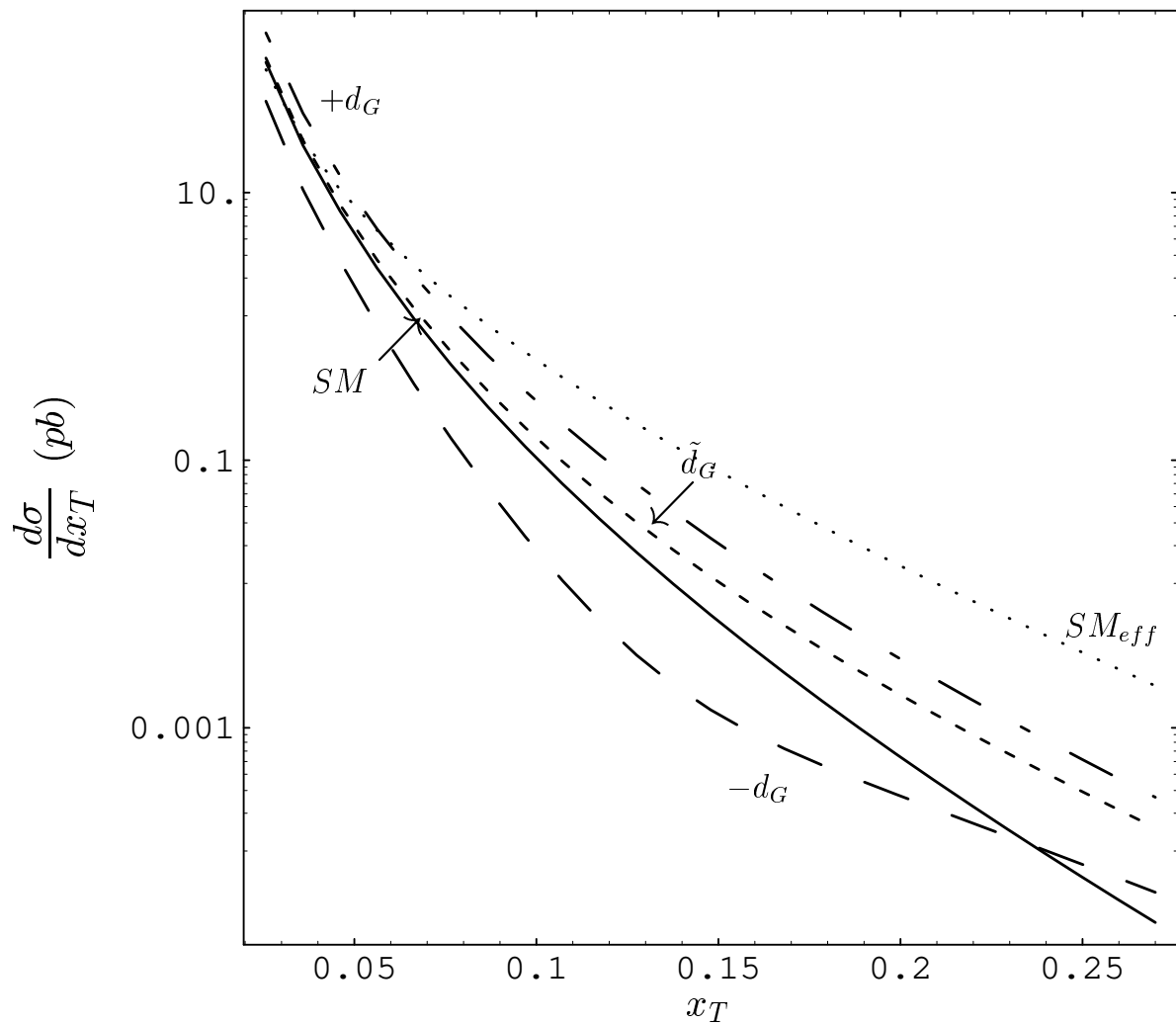


Fig. 6

Transverse energy distribution in $p + p \rightarrow H + \text{jet} + X$ at LHC. See caption of Fig.4.

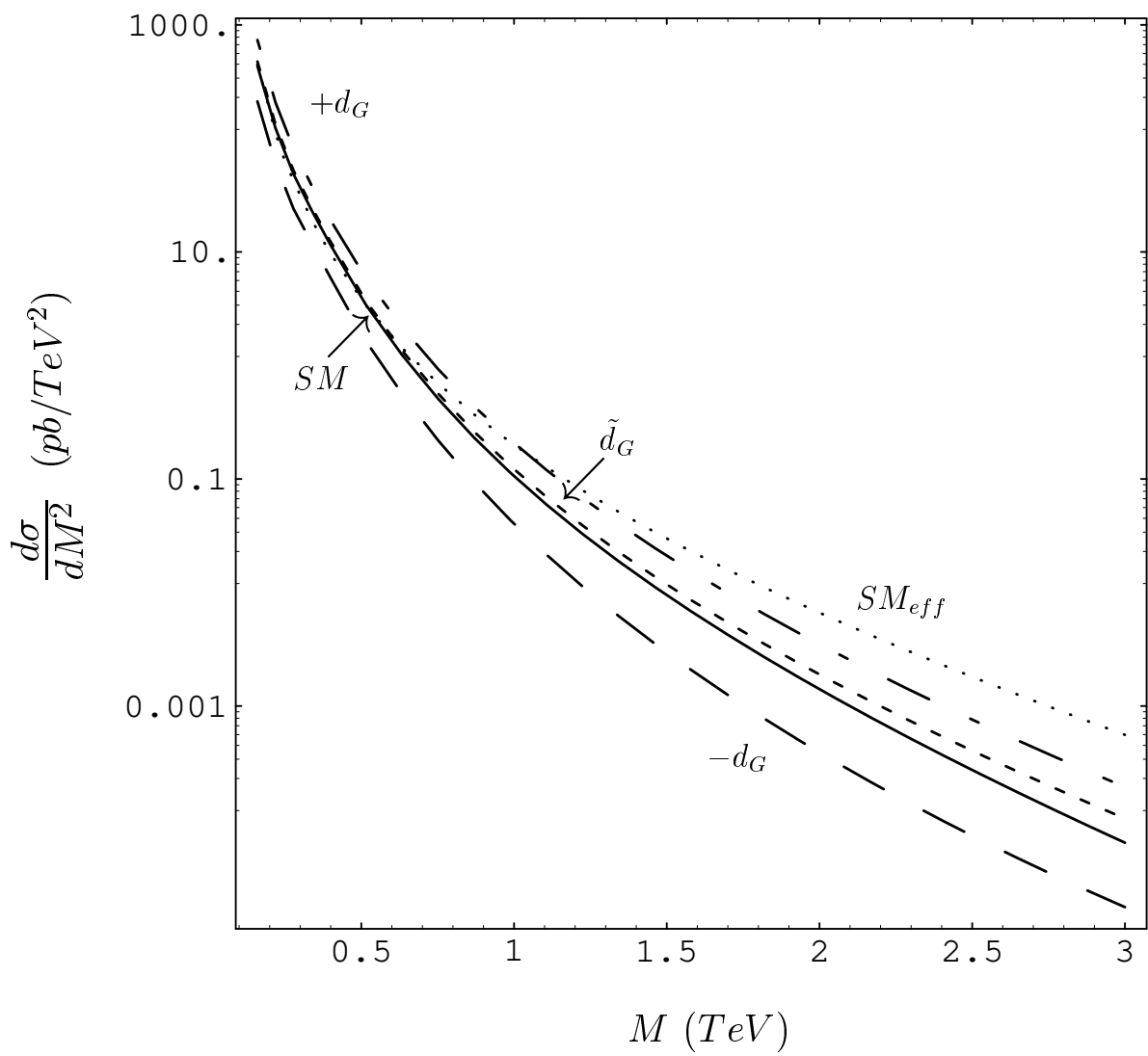


Fig. 7

Invariant mass distribution in $p + p \rightarrow H + \text{jet} + X$ at LHC. See caption of Fig.4.